# Physics-model-based Control of the Plasma Current Profile Dynamics for the Development and Sustainment of Advanced Scenarios in DIII-D

J.E. Barton 1), M.D. Boyer 1,2), W. Shi 1), W.P. Wehner 1), E. Schuster 1), J.R. Ferron 3), M.L. Walker 3), D.A. Humphreys 3), T.C. Luce 3), B.G. Penaflor 3), and R.D. Johnson 3)

1) Lehigh University, Bethlehem, Pennsylvania 18015-3085, USA.
2) Oak Ridge Institute for Science Education, Oak Ridge, Tennessee 37830-8050, USA.
3) General Atomics, PO Box 85608, San Diego, California 92186-5608, USA.

e-mail contact of main author: justin.barton@lehigh.edu

**Abstract.** DIII-D experimental results are reported to demonstrate the potential of physics-model-based $q$-profile control for robust and reproducible sustainment of advanced scenarios. In the absence of feedback control, variability in wall conditions and plasma impurities, as well as drifts due to external disturbances, can limit the reproducibility of discharges with simple pre-programmed scenario trajectories. The control architecture utilized is a feedforward + feedback scheme where the feedforward commands are computed off-line and the feedback commands are computed on-line. Good agreement between experimental results and simulations demonstrates the accuracy of the models employed for physics-model-based control design. Additionally, the results indicate the need for integrated $q$-profile and normalized beta ($\beta_N$) control to further enhance the ability to achieve robust scenario execution, which is a subject of ongoing work.

## 1. Introduction

Control of the safety factor profile ($q$-profile), and its eventual integration with normalized beta ($\beta_N$) control, have the potential to improve the ability to robustly achieve target plasma scenarios. Experimental results are reported to demonstrate the $q$-profile control capabilities in DIII-D. The $q$-profile is a key plasma property investigated in the development of advanced tokamak scenarios due to the close relationship the $q$-profile has to plasma transport (affects bootstrap current-drive, auxiliary current-drive, and fusion gain) and stability limits that are approached by increasing the plasma pressure. Due to this complex set of interactions, as well as variability in the plasma response, impurities, and drifts due to external disturbances, the problems of predicting (using models) and achieving (in experiments) advanced scenarios are extremely challenging. This motivates the design of feedforward + feedback controllers, which are derived by embedding the known physics of the plasma (described by relevant models) into the design process through *model-based* design techniques, to regulate plasma conditions. As a result of the embedded physics, model-based controllers know in which direction to actuate to generate a desired plasma response and can be designed to share the available actuation capabilities. The ability to robustly achieve and maintain target plasma states through feedback can enable the study of desired regimes, control the proximity to stability limits, and maximize the physics output of the executed discharges. The reported results show the potential of physics-model-based controllers to meet these demanding challenges.

To develop model-based controllers, control-oriented models that describe the plasma response to the actuators, such as the auxiliary heating and current-drive (H&CD) system, must first be developed. The control-oriented models can be obtained through either data-driven (DD) or first-principles-driven (FPD), physics-based modeling techniques. Advances in developing models/profile-control-strategies following a DD approach are discussed in [1–3]. The foundation of FPD models, which are employed in this work, are the fundamental physical laws that govern the evolution of the plasma, such as the poloidal magnetic flux diffusion equation. The goal in the development of FPD models is the conversion of these accepted physics models into a form *suitable for control design*. Where first-principles knowledge of a plasma parameter is either too complex for control design or not fully understood, such as the plasma thermal

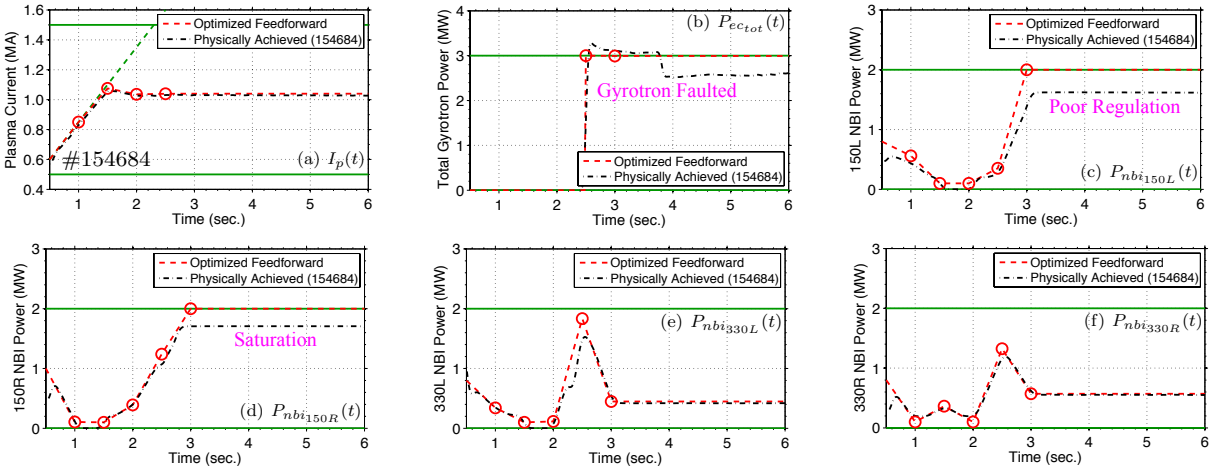


*FIG. 1. Optimized and physically achieved (DIII-D shot 154684) actuator trajectories: (a) total plasma current, (b) total EC power (set to be inactive during the time interval $t \in [0.5, 2.5)$ s because of the limited amount of total energy the gyrotrons can deliver in one discharge), and (c-f) individual NBI powers. Actuator limitations (either in regulation or faults) are indicated in the respective figures. Additionally, the actuator magnitude (solid green) and rate (dash green) limits applied on the optimization problem solution are also shown. The actuator trajectories are represented by a finite number of parameters (red ○) and the associated actuator trajectories (red - - line) are determined by linear interpolation during the time intervals between the individually optimized parameters.*

conductivity, general physical observations and experimental/simulated data are used to close the physics model by developing a simplified model of the plasma parameter in question, thereby obtaining a *first-principles-driven, physics-based* model. Progress towards modeling the plasma dynamics following a FPD approach in low performance (L-mode) [4–6] and high performance (H-mode) [7] scenarios has been recently reported. Experiments at DIII-D [8–10] represent the first successful demonstration of FPD closed-loop $q$-profile control (in L-mode scenarios) in a tokamak device. In this work, the control philosophy employed in [8–10] is extended to H-mode scenarios in DIII-D by developing a systematic approach to scenario planning through the design of a numerical optimization algorithm to synthesize feedforward actuator trajectories [11] and feedback controllers to actively control the $q$-profile [12, 13].

## 2. Overview of Control Architecture and Modeling Philosophy

The utilized control scheme can be designed to more heavily weight particular regions of interest of the $q$-profile relative to others, and therefore, can be readily tailored to suit the needs of various physics experiments. The employed control architecture is a feedforward + feedback scheme where the feedforward commands are computed off-line and the feedback commands are computed on-line. At the core of the control algorithms is a nonlinear, physics-based, control-oriented model that captures the response of the plasma ($q$-profile and $\beta_N$) to the control actuators (total plasma current ($I_p$), line average electron density ($\bar{n}_e$), auxiliary electron cyclotron (EC) power ($P_{ec}$), and auxiliary neutral beam injection (NBI) power ($P_{nbi}$)). The auxiliary H&CD actuators on DIII-D considered in this work are 6 gyrotrons, which are grouped together to form 1 effective EC source for control, and 6 individual co-current NBI sources, which are referred to by the names [30L/R,150L/R,330L/R], where L and R denote left and right lines, respectively. In the H&CD scheme considered, the EC source and the 150L/R NBI lines are utilized as off-axis H&CD sources, while the 30L/R and 330L/R NBI lines are utilized as on-axis H&CD sources.

The evolution of the poloidal magnetic flux profile, which is related to the $q$-profile, is given by the magnetic diffusion equation [14]

$$\frac{\partial \psi}{\partial t} = \frac{\eta(T_e)}{\mu_0 \rho_b^2 \hat{F}^2} \frac{1}{\hat{\rho}} \frac{\partial}{\partial \hat{\rho}} \left( \hat{\rho} \hat{F} \hat{G} \hat{H} \frac{\partial \psi}{\partial \hat{\rho}} \right) + R_0 \hat{H} \eta(T_e) \left[ j_{aux} + j_{bs} \right], \tag{1}$$

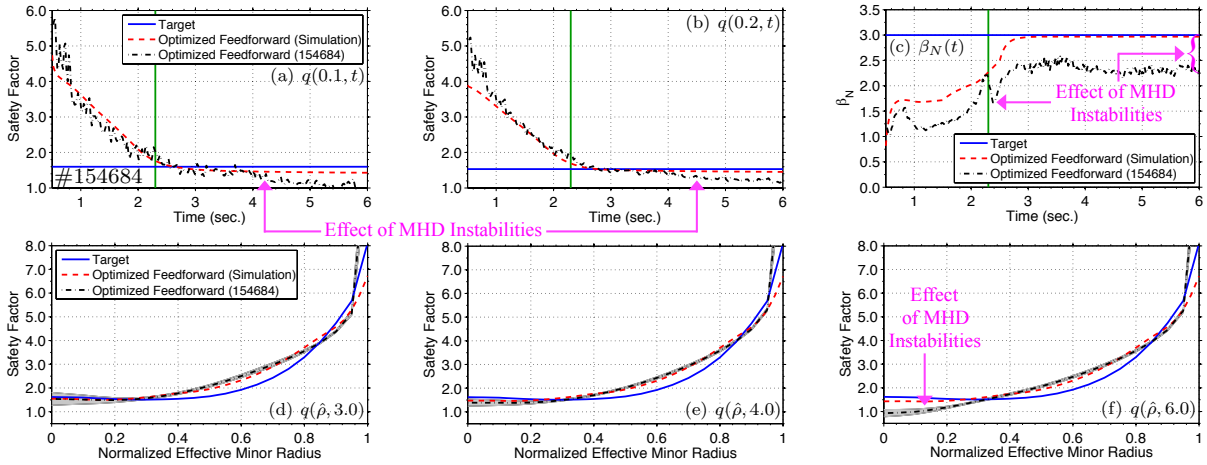


*FIG. 2. Simulated and experimental (DIII-D shot 154684) testing of optimized actuator trajectories: (a-b) time traces of $q$ at $\hat{\rho} = 0.1$ and 0.2, (c) time trace of $\beta_N$, and (d-f) $q$-profile at $t = 3.0, 4.0$, and 6.0 $s$. The solid green line denotes the onset of MHD instabilities during DIII-D shot 154684. Approximate error bars for the measured $q$-profiles (obtained from rtEFIT [15]) are shown by the gray-shaded regions.*

with boundary conditions $(\partial\psi/\partial\hat{\rho})|_{\hat{\rho}=0} = 0$ and $(\partial\psi/\partial\hat{\rho})|_{\hat{\rho}=1} = -k_{I_p} I_p(t)$, where $\psi$ is the poloidal stream function, which is closely related to the poloidal magnetic flux $\Psi$ ($\Psi = 2\pi\psi$), $t$ is the time, $\eta$ is the plasma resistivity, $T_e$ is the electron temperature, $\mu_0$ is the vacuum magnetic permeability, $j_{aux}$ and $j_{bs}$ are the current density driven by auxiliary sources and the bootstrap effect, respectively, and $k_{I_p}$ is a constant. The spatial coordinate $\hat{\rho} = \rho/\rho_b$ (normalized effective minor radius) indexes the plasma magnetic flux surfaces, where $\rho$ is the effective minor radius of a magnetic flux surface, i.e., $\Phi(\rho) = \pi B_{\phi,0}\rho^2$, $\Phi$ is the toroidal magnetic flux, $B_{\phi,0}$ is the vacuum toroidal magnetic field at the geometric major radius $R_0$ of the tokamak, and $\rho_b$ is the effective minor radius of the last closed magnetic flux surface. The parameters $\hat{F}(\hat{\rho})$, $\hat{G}(\hat{\rho})$, $\hat{H}(\hat{\rho})$, and $k_{I_p}$ are geometric factors pertaining to the magnetic configuration of a particular plasma equilibrium. A FPD model of the evolution of the poloidal flux profile, and hence the $q$-profile ($q(\hat{\rho},t) = -\mathrm{d}\Phi/\mathrm{d}\Psi = -(B_{\phi,0}\rho_b^2\hat{\rho})/[\partial\psi/\partial\hat{\rho}]$), is developed by combining (1) with physics-based models of the electron density, the electron temperature, the plasma resistivity, and the noninductive current sources [7]. The evolution of the plasma internal energy, which is related to $\beta_N$, is modeled by a volume-averaged energy balance equation. The physics information contained in the nonlinear model is embedded into the feedforward and feedback components of the control scheme through advanced model-based control design techniques.

## 3. Scenario Planning by Feedforward Actuator Trajectory Optimization

### A Design Methodology and Optimization Problem Formulation

The objective of the actuator trajectory optimization algorithm is to design actuator waveforms that steer the plasma from a particular initial condition through the tokamak operating space to reach a target state at some time $t_f$ during the discharge. One of the key physics goals of plasma profile control is to reach a target plasma state at a desired time and maintain that state to enable the study of desired regimes and make the best use of the discharge. The target state is chosen to be defined in terms of a desired $q$-profile and $\beta_N$, as well as a constant loop-voltage profile to ensure the plasma remains at the desired operating point. The proximity of the achieved plasma state to the predefined target is formulated into a cost functional ($J$) [11]. Actuator and plasma state/magnetohydrodynamic-stability (MHD-stability) constraints are imposed as limitations on the optimization problem solution. The actuator constraints are the maximum amount of auxiliary H&CD power and the total plasma current ramp rate. The plasma state/MHD-stability constraints are the minimum allowable $q$-value ($q_{min}$), i.e., $q_{min}$ must be $\geq 1$ to avoid sawtooth

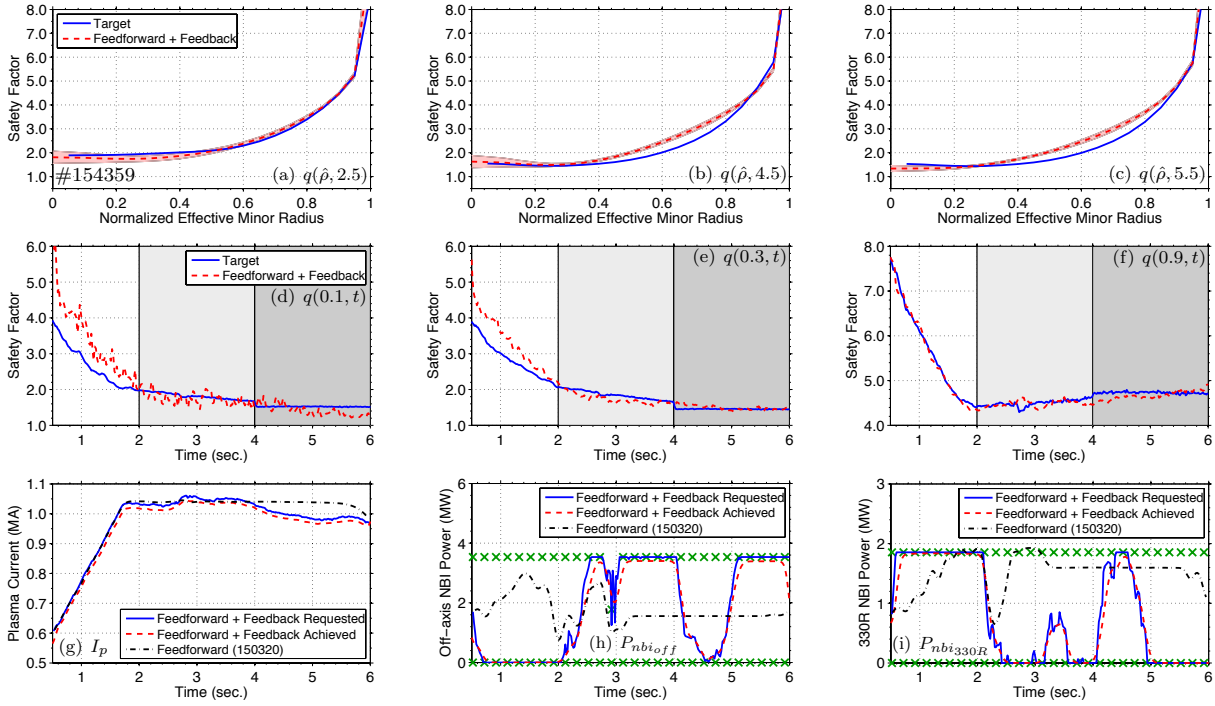


*FIG. 3. Experimental testing of q-profile feedback controller during DIII-D shot 154359: (a-c) q-profile at $t = 2.5, 4.5,$ and 5.5 s, (d-f) time traces of $q$ at $\hat{\rho} = 0.1, 0.3,$ and 0.9, and (g-i) comparison of actuator trajectories ($P_{nbi_{off}} = P_{nbi_{150L}} + P_{nbi_{150R}}$). Approximate error bars for the measured q-profiles (obtained from rtEFIT [15]) are shown by the red-shaded regions. Note: actuator limits denoted by green X.*

oscillations, the net power across the plasma surface must be greater than the H-mode threshold power to ensure the plasma remains in the H-mode operating regime, and the line average electron density must be lower than the Greenwald density limit. The nonlinear, constrained optimization problem is then to design actuator trajectories that minimize $J$ subject to the plasma dynamics (governed by the physics-based model prediction [7]) and constraints [11].

## B Design and Experimental Testing of Optimized Feedforward Trajectories

The optimized actuator trajectories determined by solving the optimization problem using a method called sequential quadratic programming [16], with the target plasma state chosen to be the $q$-profile and $\beta_N$ experimentally achieved at 3.0 s in DIII-D shot 150320, are shown in Fig. 1 [11]. The optimization is carried out over the time interval $t_{opt} = t \in [t_0, t_f] = [0.5, 3.0]$ s. Firstly, the total plasma current is ramped up at the maximum allowable rate, which is set to avoid triggering tearing modes due to a loss of magnetic shear near the plasma boundary, and exhibits a slight overshoot before settling to the specified final value. Secondly, the off-axis NBI power ($P_{nbi_{150L/R}}$) is gradually increased up to the maximum allowable value during the time interval $t \in [1.5, 3]$ s to set up a stationary plasma state with off-axis auxiliary current-drive, which is needed to achieve the target $q$-profile in the plasma core. Thirdly, the maximum amount of EC power is injected into the plasma with the same objective as well as to reach the target $\beta_N$. Finally, a moderate amount of on-axis NBI power ($P_{nbi_{330L/R}}$) is injected into the plasma during the time interval $t \in [2, 3]$ s to set up a stationary state before settling to a relatively small amount that is needed to achieve the target $\beta_N$. In order to acquire diagnostic data to reconstruct the $q$-profile, the 30L/R NBI powers are fixed at a constant 1.1 MW. The line average electron density trajectory is chosen to be fixed (linearly ramped up from an initial value $\bar{n}_e(0.5) = 2 \times 10^{19}$ m$^{-3}$ to a final value $\bar{n}_e(2.0) = 4.2 \times 10^{19}$ m$^{-3}$ and then held constant) because density control is challenging in experiments due to large particle recycling at the tokamak wall.

The actuator trajectories shown in Fig. 1 were tested through simulation with the physics-based model of the plasma dynamics [7] and experimentally in DIII-D during shot 154684 [11].

As the optimized trajectories were designed to achieve a target plasma state at the time $t_f = 3.0$ s in such a way that the achieved state is as stationary in time as possible, the actuator values were held constant from the time $t_f$ until the end of the discharge. It is important to note that the optimized trajectories represent the references to the dedicated control loops that command the DIII-D physical actuators, and as shown in Fig. 1, the dedicated control loops were able to follow the requested trajectories reasonably well. Time traces of $q$ at various radial locations and of $\beta_N$, and a comparison of the target, physics-based model predicted, and experimentally achieved $q$-profiles at various times is shown in Fig. 2. As illustrated, the optimized trajectories were able to drive the experimental plasma as close as possible to the desired stationary $q$-profile at 3.0 s. However, at 2.3 s, MHD instabilities developed and persisted for the remainder of the discharge. The MHD instabilities degraded the plasma confinement characteristics (shown in the immediate reduction of $\beta_N$ once the modes develop) and resulted in the inability to experimentally achieve the target $\beta_N$ and maintain the target $q$-profile in the plasma core after 4.0 s. However, through simulation with the physics-based model, it was shown that the optimized trajectories were able to steer the simulated plasma to the stationary target in the absence of MHD modes. Finally, note the good agreement between the simulated and experimental $q$-profile evolution during the time interval $t \in [0.5, 4.0]$ s, which provides confidence in the ability of the physics-based model to satisfactorily predict the evolution of the plasma for control algorithm design purposes.

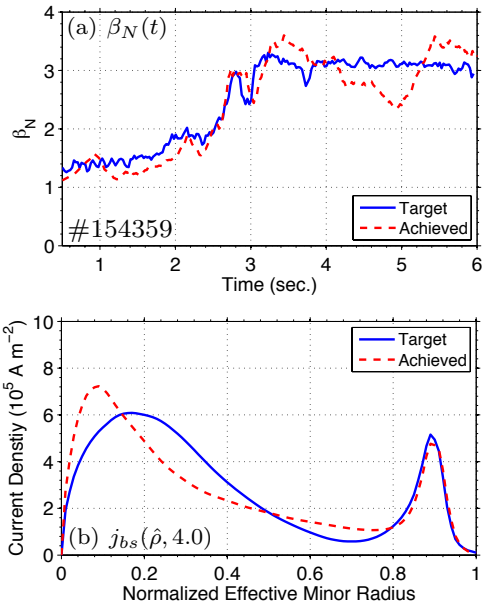


*FIG. 4. Comparison of (a) $\beta_N$ and (b) bootstrap current profile (computed by TRANSP [17]) at 4.0 s. The bootstrap fraction in the target discharge was $f_{bs} = 38\%$ and in the feedback-controlled discharge was $f_{bs} = 39\%$ at 4.0 s.*

### C Discussion and Implications of Optimized Actuator Trajectory Testing Results

As a result of the MHD instabilities that developed during the experimental test of the optimized trajectories, the target $\beta_N$ was not able to be achieved and the target $q$-profile was unable to be maintained in a stationary condition. Therefore to compensate for external disturbances (such as a reduction in confinement) and actuation limitations (either in regulation or faults), the feedforward trajectories need to be integrated together with a feedback control scheme, as discussed in the next section, to improve the ability to robustly achieve plasma target conditions.

## 4. Physics-model-based Feedback Control Design

### A Robust Control Design Methodology

We begin the feedback control design process by modeling the evolution of the electron density, the electron temperature, and the plasma resistivity each as a nominal profile plus a bounded uncertain profile. These uncertain models and the noninductive current-drive models [7] are combined with the magnetic diffusion equation (1) to yield a FPD model suitable for control design. The physics information contained in the model is embedded into the feedback controller by employing *robust control design* techniques [18]. The controller is designed for tighter regulation of the $q$-profile in the spatial regions $\hat{\rho} \in (0, 0.3]$ and $\hat{\rho} \in [0.85, 1)$, as the $q$-value in these regions intimately affects plasma stability and performance. Additionally, the controller is designed to maintain closed-loop system stability in the presence of the uncertainty, which provides confidence that the controller can be utilized in a variety of operating conditions [12].

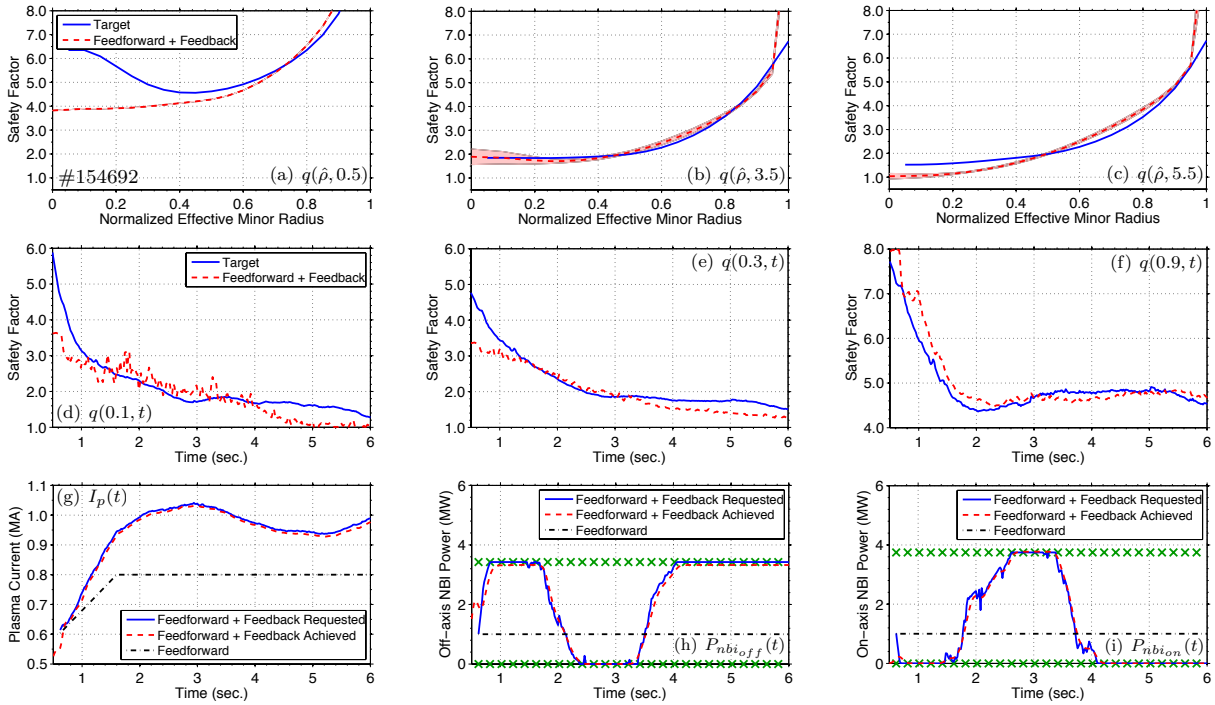


*FIG. 5. Experimental testing of q-profile feedback controller during DIII-D shot 154692: (a-c) q-profile at $t = 0.5, 3.5$, and 5.5 s, (d-f) time trace of $q$ at $\hat{\rho} = 0.1, 0.3$, and 0.9, and (g-i) comparison of actuator trajectories ($P_{nbi_{on}} = P_{nbi_{330L}} + P_{nbi_{330R}}$). Approximate error bars for the measured q-profiles (obtained from rtEFIT [15]) are shown by the red-shaded regions. Note: actuator limits denoted by green X.*

## B Feedforward + Feedback Testing: Reference Tracking Experiment

In a DIII-D discharge, robust tracking of a stationary target $q$-profile was obtained in the presence of external plasma disturbances. In DIII-D shot 154359, a $q$-profile feedback controller [12] (not including $\beta_N$ feedback control) was tested in a feedforward + feedback target tracking experiment. The target $q$-profile ($q^{tar}(\hat{\rho}, t)$) was obtained from the $q$-profile achieved in DIII-D shot 150320 ($q^{320}(\hat{\rho}, t)$) as follows: $q^{tar}(\hat{\rho}, t) = q^{320}(\hat{\rho}, t)$ over $t \in [0.5, 2.0]$ s, $q^{tar}(\hat{\rho}, t) = q^{320}(\hat{\rho}, 2) + \left[q^{320}(\hat{\rho}, 5) - q^{320}(\hat{\rho}, 2)\right](t-2)/(5-2)$ over $t \in (2.0, 4.0)$ s, and $q^{tar}(\hat{\rho}, t) = q^{320}(\hat{\rho}, 5.0)$ over $t \in [4.0, 6.0]$ s. The feedforward component of the control input was chosen to be the actuator trajectories achieved in DIII-D shot 150320. A second key physics goal of plasma profile control is to be able to robustly reproduce target scenarios and enable controlled variation of specific characteristics of the profiles through feedback to better elucidate physics.

A comparison of the target and experimentally achieved $q$-profiles at various times, time traces of $q$ at various radial locations, and a comparison of the actuator trajectories is shown in Fig. 3. As illustrated, the controller was able to drive the $q$-profile to the target (specifically in the spatial regions where the tracking performance was more heavily weighted ($\hat{\rho} \in (0, 0.3]$ and $\hat{\rho} \in [0.85, 1.0)$)) and achieve a relatively stationary condition in the presence of perturbations in the initial conditions and actuator regulation disturbances. During the feedback-controlled discharge, the 30L/R NBI lines were utilized at a constant power (total of 2 MW) to acquire diagnostic data while during the target discharge the power in these beams was increased from a low value (total of 1.2 MW) to a high value (total of 3.2 MW) at 3.0 s. Also, during the feedback-controlled discharge, the 330L NBI line and the EC launchers were unavailable for feedback control. The controller utilized the total plasma current to regulate the $q$-profile near the plasma boundary (Figs. 3(f) and 3(g)) and modulated the mix of the on-and-off axis auxiliary current-drives that were available for feedback control to track the target $q$-profile in the plasma core (Figs. 3(d-e) and 3(h-i)). Finally, as shown in Fig. 4(a), the achieved $\beta_N$ was relatively close to the target even though it was not feedback-controlled. This resulted in a similar bootstrap current profile in both the target and feedback-controlled discharges as shown in Fig. 4(b).

### C Pure Feedback Testing: Disturbance Rejection Experiment

In another DIII-D discharge, rejection of disturbances in the initial $q$-profile was obtained. In DIII-D shot 154692, a $q$-profile feedback controller [12] (not including $\beta_N$ feedback control) was tested in a pure feedback disturbance rejection experiment. The $q$-profile evolution achieved in DIII-D shot 154358 was chosen as the target. A significant disturbance (low relative to the target) in the $q$-profile at 0.5 s (when the feedback controller was turned on) was introduced to the plasma by delaying the H-mode transition time. The feedforward component of the control input was frozen after 1.6 s, therefore, the achieved profile regulation was obtained exclusively through feedback. Another important goal of profile control experiments is to investigate the minimum number of variables that must be controlled to achieve robust scenario execution.

A comparison of the target and experimentally achieved $q$-profiles at various times, time traces of $q$ at various radial locations, and a comparison of the actuator trajectories is shown in Fig. 5. As shown in the figures, the controller was able to reject the effects of the initial condition error and drive the $q$-profile to the target during the time interval $t \in [0.5, 3.5]$ s in the presence of actuator regulation disturbances (gyrotrons unavailable for feedback control). The controller utilized the actuators to regulate the $q$-profile across the spatial domain in the same way as in the previously discussed feedback experiment (Figs. 5(d-i)). However, even though the controller requested the maximum amount of off-axis auxiliary current-drive during the time interval $t \in [4.0, 6.0]$ s, the $q$-profile in the plasma core was unable to be maintained at the target. As shown in Fig. 6(a), the achieved $\beta_N$ was relatively far away from the target during the time interval $t \in (3.0, 5.5]$ s. This resulted in a lower bootstrap current profile in the feedback-controlled discharge relative to the target as shown in Fig. 6(b). As the bootstrap current is an off-axis source of current, a lower bootstrap current may have contributed to the inability to maintain the $q$-profile in the plasma core at the target during the feedback-controlled experiment.

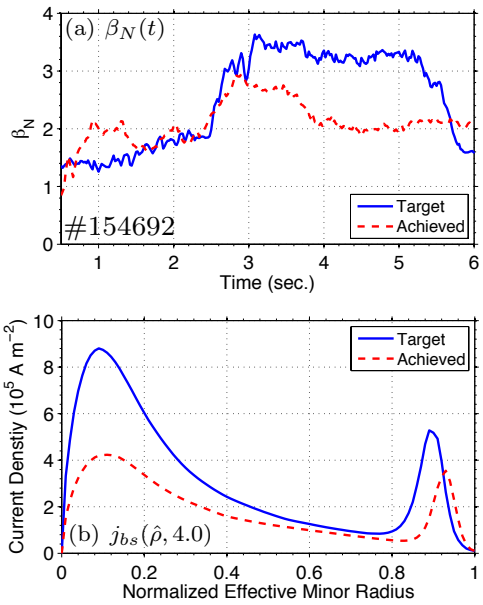


*FIG. 6. Comparison of (a) $\beta_N$ and (b) bootstrap current profile (computed by TRANSP [17]) at 4.0 s. The bootstrap fraction in the target discharge was $f_{bs} =$ 39% and in the feedback-controlled discharge was $f_{bs} = 27\%$ at 4.0 s.*

## 5. Conclusions and Discussion

The reported advances demonstrate the potential physics-model-based profile control has to provide a systematic approach for the development and robust sustainment of advanced scenarios in DIII-D. These control algorithms also enable detailed study of the accuracy and validity of the relevant models themselves and can help clarify physics aspects important to robust scenario execution. As observed in the experimental test of the optimized trajectories, access to advanced scenarios can be limited by triggering MHD instabilities. Therefore, one direction of future work is to formulate additional plasma state constraints that can be imposed on the optimization problem solution to maintain distance from critical MHD stability limits, such as classical and neoclassical tearing modes. A second direction of future work is to extend the physics-based model by coupling the poloidal magnetic flux profile dynamics together with the distributed dynamics of the electron temperature profile in order to better represent the effect the $q$-profile has on plasma transport [19]. The $q$-profile feedback control experiments indicate that another important aspect to achieving robust scenario execution is the need to simultaneously achieve a target $q$-profile and $\beta_N$, which is a subject of ongoing work [12]. The development of these profile control capabilities may not only help achieve physics objectives on DIII-D, but will

also help evaluate a control scheme that potentially can be utilized in future experiments and fusion power plants. The control scheme developed in this work is readily adaptable to a given operating scenario in a given machine of interest due to the strong first-principles dependence of the modeling and design approach used to synthesize controllers. The developed feedforward + feedback scheme has been employed to improve the reproducibility of plasma startup conditions on DIII-D by achieving a specified target $q$-profile at the end of the current ramp-up phase [20]. Additionally, feedback algorithms for profile control have been developed for simultaneous tracking of $q$-profile and $\beta_N$ targets in ITER H-mode scenarios [21], and tracking of $q$-profile targets in NSTX-U H-mode scenarios [22] and in TCV L-mode scenarios [23].

This material is based upon work partly supported by the U.S. Department of Energy, Office of Science, Office of Fusion Energy Sciences, using the DIII-D National Fusion Facility, a DOE Office of Science user facility, under Awards DE-SC0001334, DE-SC0010661, DE-AC05-00OR23100, and DE-FC02-04ER54698.

## References

[1] SHI, W. et al., A Two-time-scale Model-based Combined Magnetic and Kinetic Control System for Advanced Tokamak Scenarios on DIII-D, in *51st IEEE Conference on Decision and Control*, pp. 4347–4352, 2012.

[2] WEHNER, W. et al., Identification and Control of Magneto-Kinetic Response During Advanced Tokamak Scenarios in DIII-D, in *2013 American Control Conference*, pp. 1219–1224, 2013.

[3] MOREAU, D. et al., Nuclear Fusion **53** (2013) 063020.

[4] OU, Y. et al., Fusion Eng. Des. **82** (2007) 1153.

[5] WITRANT, E. et al., Plasma Phys. and Control. Fusion **49** (2007) 1075.

[6] FELICI, F. et al., Nuclear Fusion **51** (2011) 083052.

[7] BARTON, J. E. et al., Physics-based Control-oriented Modeling of the Safety Factor Profile Dynamics in High Performance Tokamak Plasmas, in *52nd IEEE Conference on Decision and Control*, pp. 4182–4187, 2013.

[8] BARTON, J. E. et al., Nucl. Fusion **52** (2012) 123018.

[9] BOYER, M. D. et al., Plasma Phys. Control. Fusion **55** (2013) 105007.

[10] BOYER, M. D. et al., IEEE Trans. Control Syst. Technol. **22** (2014) 1725.

[11] BARTON, J. E. et al., Nonlinear Physics-model-based Actuator Trajectory Optimization for Advanced Scenario Planning in the DIII-D Tokamak, in *19th IFAC World Congress*, pp. 671–76, 2014.

[12] BARTON, J. E. et al., Experimental and Simulation Testing of Physics-model-based Safety Factor Profile and Internal Energy Feedback Controllers in DIII-D Advanced Tokamak Scenarios, in *19th IFAC World Congress*, pp. 5223–5228, 2014.

[13] BOYER, M. D. et al., Simultaneous Boundary and Distributed Feedback Control of the Current Profile in H-mode Discharges on DIII-D, in *19th IFAC World Congress*, pp. 1568–1573, 2014.

[14] HINTON, F. and HAZELTINE, R., Rev. Mod. Phys. **48** (1976) 239.

[15] FERRON, J. R. et al., Nuclear Fusion **38** (1998) 1055.

[16] NOCEDAL, J. and WRIGHT, S. J., *Numerical Optimization*, Springer, New York, 2006.

[17] HAWRYLUK, R. J. et al., An Empirical Approach to Tokamak Transport, in *Physics of Plasmas Close to Thermonuclear Conditions,* ed B. Coppi *et al.*, vol 1, pp. 19–46, 1980.

[18] SKOGESTAD, S. and POSTLETHWAITE, I., *Multivariable Feedback Control Analysis and Design*, Wiley, New York, 2005.

[19] FERRON, J. R. et al., Nuclear Fusion **51** (2011) 063026.

[20] BARTON, J. E. et al., Optimization of the Current Ramp-up Phase in DIII-D via Physics-model-based Control of Plasma Safety Factor Profile Dynamics, in *56th Annual Meeting of the APS Division of Plasma Physics*, 2014.

[21] BARTON, J. E. et al., Robust Control of the Safety Factor Profile and Stored Energy Evolutions in High Performance Burning Plasma Scenarios in the ITER Tokamak, in *52nd IEEE Conference on Decision and Control*, pp. 4194–4199, 2013.

[22] ILHAN, Z. et al., First-Principles-Driven Model-Based Optimal Control of the Current Profile in NSTX-U, in *56th Annual Meeting of the APS Division of Plasma Physics*, 2014.

[23] BARTON, J. E. et al., Closed-loop Control of the Safety Factor Profile in the TCV Tokamak, in *53rd IEEE Conference on Decision and Control*, 2014.